Carbon dioxide methanation kinetic model on a commercial Ni/Al2O3 catalyst

Isabelle Champon, Alain Bengaouer, Albin Chaise, Sébastien Thomas, Anne-Cécile Roger

Version of Record: https://www.sciencedirect.com/science/article/pii/S2212982019301799
Manuscript_6b5d1f355181a305b639b466a848a3b4

Carbon dioxide methanation kinetic model on a commercial Ni/Al_2O_3 catalyst

Isabelle Champon[1,2,3], Alain Bengaouer[1], Albin Chaise[1], Sébastien Thomas[2], Anne-Cécile Roger[2]

[1]Université Grenoble Alpes, CEA, LITEN, DTBH, SCTR, LER, 17 Avenue des martyrs, Grenoble F-38054, France

[2]ICPEES-ECPM, UMR 7515, University of Strasbourg, 25 rue Becquerel, F-67087 Strasbourg, France

[3]French Environment and Energy Management Agency, 20 avenue du Grésillé, BP 90406, F-49004, Angers Cedex 01, France

Corresponding author: alain.bengaouer@cea.fr (Alain Bengaouer)

Abstract

Intrinsic kinetic characterization of the carbon dioxide methanation was determined over a commercial 14-17 wt.% Ni/Al_2O_3 between 623 K and 723 K at atmospheric pressure in the absence of heat and mass transfer limitations. Following a Hougen-Watson formalism, both direct path (CO_2 methanation rate equation) and indirect path (Reverse Water Gas Shift rate equation + CO methanation rate equation) were described. As a first step, kinetic tests were performed operating in differential mode to evaluate the reaction rate dependence on reactants and products partial pressure at different temperatures in order to select the form of each reaction rate equation. Kinetic models available in the literature were evaluated and compared with the experimental results and model adaptations were proposed to identify the kinetic laws that fit the best the experimental values. Kinetic and adsorption parameters were calculated from these laws. Then, the identified parameters were adjusted simultaneously on experimental tests from 5% to 75% CO_2 conversion using an isothermal plug-flow reactor. The three reaction rates and their reverse reactions were identified in order to minimize the error on CO_2 conversion and CH_4 and CO selectivities at 623 K, 673 K and 723 K. The final identified kinetic model was able to reflect the kinetics from differential conversion to thermodynamic equilibrium with an accuracy of 20% on the CH_4 formation rate for the three temperatures.

Keywords: carbon dioxide, methanation, Power-to-Gas, intrinsic kinetics, Ni/Al_2O_3 catalyst

1. Introduction

The CO_2 methanation reaction is of great interest today in the case of Power-to-Gas technologies [1–7]. Actually this reaction, also called the Sabatier reaction [8], produces Substitute Natural Gas (SNG) and enables the CO_2 valorization (from biomass or industrial flux gases for instance) in order to reduce the greenhouse gas emissions. Moreover, Power-to-Gas is known as one of the solutions to store the excess and intermittent electricity production from renewable energy [4]. Hydrogen is first synthetized by water electrolysis, and then combined with carbon dioxide to produce methane and water. Thereafter, methane can be injected in the gas grid and is more easily stored than hydrogen. It can be transported *via* the gas grid, and be used in a great variety of end-use applications (heat, mobility, *etc.*) [4].

The CO_2 hydrogenation into CH_4 (reaction (1)) is balanced, highly exothermic, favored at low temperatures and high pressures.

As reactions in gas phase are extremely slow at moderate temperatures and pressures, a catalyst is needed to obtain an acceptable reaction rate and methane selectivity [5]. Supported catalysts are widely used to perform CO_2 methanation. Usually, they are composed of a metallic active phase (Ni, Ru, Rh, Co), dispersed on an oxide support (Al_2O_3, CeO_2, SiO_2, *etc.*). Nickel based catalysts supported on alumina are the most largely employed because of their high performance/cost ratio [3].

The CO_2 methanation can also be a combination of Reverse Water Gas Shift (RWGS) and CO methanation (balanced reactions (2) and (3)) [9].

$$CO_2 + 4H_2 \rightleftharpoons CH_4 + 2H_2O \qquad \Delta_r H^0_{298\,K} = -165\ kJ.mol^{-1} \qquad (1)$$

$$CO_2 + H_2 \rightleftharpoons CO + H_2O \qquad \Delta_r H^0_{298\,K} = 41\ kJ.mol^{-1} \qquad (2)$$

$$CO + 3H_2 \rightleftharpoons CH_4 + H_2O \qquad \Delta_r H^0_{298\,K} = -206\ kJ.mol^{-1} \qquad (3)$$

Several authors have studied the CO and CO_2 methanation kinetics. Some studies use a simple power rate law [10–12]. However, more rigorous models result from reaction mechanism considerations and follow the Hougen Watson formalism. A recent review introduced exhaustively the CO and CO_2 methanation kinetics [6].

Xu and Froment [13] proposed three reaction rates on a 15.2 wt.% Ni/$MgAl_2O_4$ catalyst, derived from methane steam reforming, CO_2 methanation and reverse water gas shift experiments. Experimentally, the fixed-bed reactor was operated in integral mode (reaction rates cannot be considered as constant along the catalyst bed) with 400.0 mg of commercial catalyst diluted with α-alumina. The data used for the kinetic study were recorded after 70 h on stream to stabilize its activity. The conditions of the experiments were 573 to 673 K, 300 to 1000 kPa and 6 to 30 ml (STP) min^{-1}. They employed a Marquardt routine to estimate the kinetic parameters by minimization of the sum of weighted residual squares of the conversions, the latter being calculated by the fourth-order Runge-Kutta routine. Finally, they identified 14 parameters: activation energies and pre-exponential factors of the 3 kinetic constants corresponding to the three reactions (Eqs (1), (2), and (3)), following an Arrhenius law and heat of adsorption and pre-exponential factors of 4 adsorption constants, as Van't Hoff-type. However, they obtained a negative heat of adsorption for water, which has no physical meaning.

Ducamp *et al*. [14] proposed a kinetic model based on the Xu and Froment kinetic formalism and adjusted on 15.0-26.0 mg of a commercial 17 wt.% Ni/Al_2O_3 catalyst diluted in SiC and operating in integral mode. The conditions of the experiments were 553 to 673 K, 100 to 1000 kPa and 120 – 125 ml (STP) min^{-1} in stoichiometric conditions for the CO_2 methanation and in hydrogen excess for the CO methanation – in order to slow down the catalyst deactivation. Only the three kinetic constants and the CO adsorption constant were identified. All other constants were unchanged, even if the two catalysts were different and if the water heat of adsorption was negative.

Weatherbee and Bartholomew [15] measured the rate of CO_2 hydrogenation on 300.0 mg of a 3 wt.% Ni/SiO_2 catalyst, between 500 and 600 K, 140 to 175 kPa, and 500 to 1500 ml (STP) min^{-1}. The CO_2 conversion was limited to 10%, so the reactor was operated in differential mode. H_2 and CO_2 partial pressure rate dependence were established. As CO was produced by the reaction (Eq (2)), some tests were performed with CO at the inlet of the reactor. The CO_2 methanation rate decreased in the presence of CO. A kinetic law for the CO_2 methanation reaction was proposed, assuming the formation of adsorbed CO which could further dissociate or desorb. Nevertheless, they neglected the CO methanation path which could also form CH_4.

Recently, Koschany *et al*. [16] studied the CO_2 methanation kinetic in differential mode considering only the direct path (Eq (1)), neglecting the reverse water gas shift reaction because the CO content in the product gas was below 1000 ppm. They prepared a co-precipitated $NiAl(O)_x$ catalyst. A mass of 25.0 to 75.0 mg of catalyst (30-90 wt.% Ni) diluted in SiC was stabilized for 300 h on stream. Temperature was varied between 453 and 523 K. Pressure was limited to 2000 kPa and flow rates were set from 45 to 75 ml (STP) min^{-1}.

Miguel *et al*. [17] determined the intrinsic kinetics of CO_2 methanation over a commercial calcium aluminate catalyst (20-25 wt.% NiO). Temperature varied between 523 and 623 K at atmospheric pressure. 12.0 to 40.0 mg of catalyst was employed for a total feed flow rates of 30-100 ml (STP) min^{-1}.

At an industrial or pilot scale, different reactor types are used (fluidized bed reactors, adiabatic or cooled fixed-bed reactors, micro-reactors, metallic-foam reactors, structured coated reactors or milli-structured fixed-bed reactors-exchangers) [6,18,19,14,20].

The purpose of this study is to develop a new kinetic model accounting for the direct (Eq (1)) and indirect paths (Eqs (2) + (3)) of the CO_2 methanation reaction with a 14-17 wt.% Ni/Al_2O_3 commercial catalyst from 623 K until 723 K at atmospheric pressure. The temperature range of this study is explained by the fact that the proposed kinetic model is intended to be used to describe the behavior of a milli-

structured fixed-bed reactor-exchanger channel. The temperatures of interest are therefore around 573 K.

2. Experimental Study

2.1. Equipment and materials

Experimental kinetic tests were performed at atmospheric pressure, between 623 K and 723 K on a 14-17 wt.% Ni/Al_2O_3 commercial catalyst. Catalyst (mass between 1.5 mg and 10.0 mg) was diluted in SiC ($4 < \Psi < 32$) in the grain size range 125 – 250 µm.

Kinetic measurements setup was divided in three parts: gas alimentation and mixing, reaction zone and analysis section. Mass flow controllers commanded the gas feeding of the six lines (H_2, N_2 – internal standard for the GC analysis, CO_2, CH_4, CO, and Ar). The pure gases were mixed together before the reaction zone and heated up using heating tapes. Liquid water was injected into a vaporization chamber by a micro-pump (GILSON - Model 321322350), and steam mingled with the gas mixture. All the tubes were heated after the vaporization chamber to avoid water condensation. A tubular furnace, constituting the reaction zone, heated the glass reactor until 773 K. The reactor was 30 cm long and 3.0 mm inner diameter. The catalyst bed was fixed with quartz wool and located inside the isothermal zone of the furnace. A thermocouple measured the temperature at the end of the catalyst bed. After the reaction zone, a cold trap condensed the water. The dry gas mixture entered the analysis zone composed by a micro gas chromatography (INFICON 3000 MICRO GC) equipped with two columns. The MS5A module was used to separate H_2, N_2, CH_4 and CO and the PPQ module to separate CH_4, CO_2 and C_2H_6 (if present). Both were equipped with TCD detectors. For one condition (temperature/flow rate), the catalyst was hold until stabilization of the conversion (45 minutes to 60 minutes) and an average of the 15 last minutes (4-5 points) was taken as the mean value of conversion.

2.2. Pretreatment of the catalyst

A step of catalyst activation under hydrogen was needed to reduce NiO into Ni° (Eq (4)):

$$NiO + H_2 \rightarrow Ni° + H_2O \quad (4)$$

A temperature-programed reduction (TPR) was realized to establish the reduction conditions. TPR was conducted with 10% H_2 in Ar with a total flow of 50 ml (STP) min^{-1}; heating rate 10 K min^{-1} - 1273 K, holding for 60 min (see Figure 1). The first reduction zone, below 673 K, was associated with the reduction of bulk NiO and the second one, above 673 K, with NiO in strong interaction with $NiAl_2O_4$. Following the industrial recommendations and in order to obtain a catalyst as stable as possible, only the bulk NiO reduction was sought by *in situ* reduction. Consequently, the reactor was heated up under a mixture 50% H_2 in N_2, with a total flow of 16 ml (STP) min^{-1} at 5 K min^{-1} until 673 K and was kept at 673 K for 1h.

Before starting the kinetic tests, the catalyst was stabilized by thermal cycling under reactive flow ($H_2/CO_2/N_2$: 74/17/9): 673 K (1h), 723 K (1h) and 748 K during one night (15 h). The repetition of the activity tests at 623 K (1h) – 673 K (1h) – 723 K (1h) showed a stable catalytic activity.

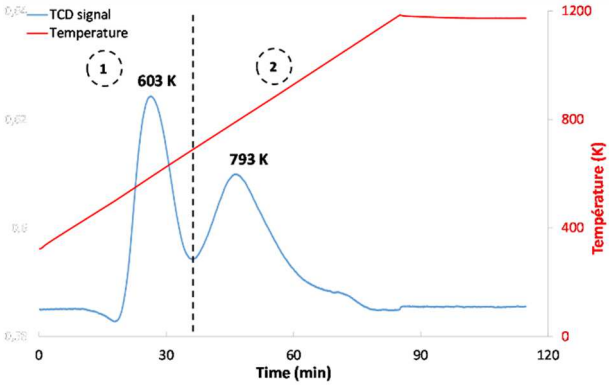

Figure 1 : Reduction profile of the commercial catalyst Ni/Al_2O_3

2.3. Diffusional limitations

Catalyst was diluted in SiC because of its thermal properties but also to increase the height of catalytic bed to obtain a plug flow reactor behavior. The plug flow assumption inside the reactor was validated

theoretically by the absence of axial dispersion ($h_{bed}/d_p > 50$ [21,22]) and radial dispersion ($d_t/d_p > 8$ [23]).The relative pressure drop over the catalyst bed was less than 20% and can be neglected [24].

To ensure the determination of the intrinsic chemical kinetics, both external and internal diffusional limitations were checked at 723 K (maximal temperature of the study). The results are presented in Figure 2.

For the verification of the absence of external transport resistances, the feed flow rate and the catalyst mass were varied, keeping the same ratio flow rate/catalyst mass (same GHSV). The CO_2 conversion obtained with catalyst mass m = 1.5 mg and flow rate Q = 27.5 ml (STP) min^{-1} was very close to the one obtained for mass 2m = 3.0 mg and flow rate 2Q = 55.0 ml (STP) min^{-1} at 673 K and 723 K and far from thermodynamic limitations (see Figure 2 (a) for a GHSV = 9.60 10^5 h^{-1}). Similarly, the CO_2 conversion obtained with catalyst mass m = 1.5 mg and flow rate Q = 41.3 ml (STP) min^{-1} was very close to the one obtained for mass 2m = 3.0 mg and flow rate 2Q = 82.5 ml (STP) min^{-1} at 723 K and far from thermodynamic limitations (see Figure 2 (a) for a GHSV = 1.44 10^6 h^{-1})

The external diffusion is promoted by the gas velocity increase, however, as similar conversions were obtained in both cases, the external diffusion can therefore be considered as not limiting for total flow rates over 27.5 ml (STP) min^{-1}.

For the internal diffusional limitations, the size of the catalyst particles was varied between 63 µm and 400 µm in several fragments by crushing and sieving: 63-125 µm, 125-250 µm, 250-315 µm, 315-400 µm. The internal limitations are well seen from CO_2 conversion obtained for 315-400 µm to 63-125 µm fractions (Figure 2 (b)). However, the relative pressure drop over the catalyst bed with 63-125 µm fraction was not negligible. Moreover, the CO_2 conversion relative gap between 125-250 µm fraction and 63-125 µm fraction is less than 7%. Hence, it was assumed that the internal diffusion was not significantly limiting for the grain size 125-250 µm, even if the transport resistance inside the grain is not zero. Thus, the kinetic study is performed with particles size between 125 and 250 µm.

Also, the theoretical heat and mass transfer limitations verifications were calculated according to the Mears-Anderson-Weisz-Prater criteria (see appendix A for details) to verify that the kinetic measurements were not affected by the mass and thermal diffusion limitations.

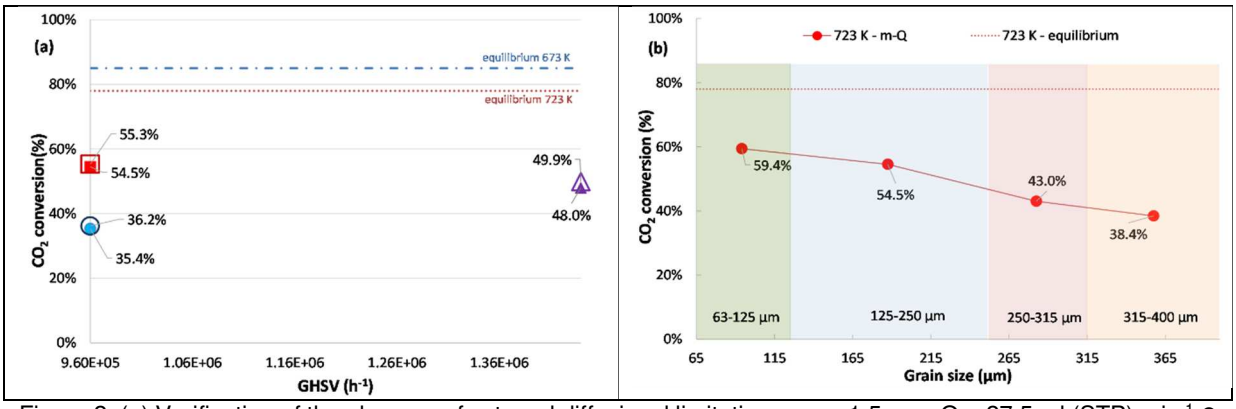

Figure 2: (a) Verification of the absence of external diffusional limitations ; m = 1.5 mg ; Q = 27.5 ml (STP) min^{-1} ● at 673 K ■ at 723 K and ▲ m = 1.5 mg and Q = 41.3 (STP) min^{-1} at 723 K compared respectively to 2m and 2Q (○, □, Δ) (b) verification of the absence of internal diffusional limitations at 723 K ; m = 1.5 mg ; Q = 27.5 ml (STP) min^{-1}

2.4. Kinetic measurements

Kinetic experiments aim at determining the reaction rate of the three reactions (Eqs (1), (2) and (3)) in a two-step procedure. First, the forms of the reaction rates are identified by low-conversion experiments with a rough estimation of their numerical parameters, which are then adjusted at higher conversion rate.

The aim of the tests at low conversion is to establish the partial pressure rate dependence of each component on each reaction, at different temperatures. To do so, the inlet partial pressure of one compound was varied while keeping the others constant. This was performed with the use of an argon flow. A maximum conversion of 20% was tolerated to assume constant reaction rate along the reactor axis. Indeed, on the basis of low conversion, the reactants partial pressure alongside the catalyst bed was assumed to be constant, and equal to the inlet values. Moreover, the reverse reactions were neglected

(far from thermodynamic limitations), and the effects of the products formed by the reactions (CO, H_2O, CH_4) were expected to be weak enough to be neglected (no chain reaction or products inhibition).

According to these assumptions, with a H_2/CO_2 flow at the reactor inlet, the CH_4 formation rate is equal to the CO_2 methanation reaction rate, and the CO formation rate equals the RWGS reaction rate:

$$r_{meth\ CO_2} = r_{CH_4}$$
$$r_{RWGS} = r_{CO}$$

With a H_2/CO flow at the inlet, the CH_4 formation rate is associated to the CO methanation reaction rate:

$$r_{meth\ CO} = r_{CH_4}$$

In order to study the influence of the products on the reaction rates, some tests were performed with a product of the possible reactions (CH_4 or H_2O) at the inlet of the reactor. To reduce the partial pressure variation alongside the catalytic bed and thus to be able to consider inlet partial pressure in the calculation, relatively high partial pressures of products were used at the reactor inlet in order to obtain $F_{products}^{\ inlet} \gg F_{products}^{\ formed}$.

Existing models from the literature were evaluated against the experimental results. They were adapted to better fit the experimental data. Finally, a first estimation of the kinetic and adsorption parameters of the three reactions were determined.

In the second set of experiments, the parameters were adjusted in order to fit experimental data at higher conversion rate. Experimentally, catalyst mass and total reactive flow rate were varied in order to reproduce the conversion rate range of an isothermal plug flow reactor. GHSV between 2.88 10^6 h^{-1} and 1.46 10^5 h^{-1} were tested at 623 K, 673 K and 723 K according to the following conditions (H_2/CO_2 = 4 and N_2 = 10% of the reactive flow rate):

- A batch of 1.5 mg of catalyst diluted in SiC ($\Psi = 32$) and a flow rate of 82.5 ml (STP) min^{-1}
- A batch of 2.0 mg of catalyst diluted in SiC ($\Psi = 24$) and three flow rates (82.5-55.0-27.5 ml (STP) min^{-1})
- A batch of 10.0 mg of catalyst diluted in SiC ($\Psi = 4$) and three flow rates (82.5-55.0-27.5 ml (STP) min^{-1}).

Numerically, an isothermal plug flow was modeled by 100 CSTR in series with the same mass of catalyst. The kinetic laws and their roughly estimated numerical parameters were employed to evaluate the partial flow rate alongside the catalytic bed with the three reactions occurring in parallel, according to the composition, flow rate and pressure at the inlet of the reactor and the conditions of temperature and catalyst mass. A linear pressure drop was assumed between the reactor inlet (around 130 kPa) and the atmospheric pressure at the outlet. The equilibrium constants of the three reactions were calculated according to the Gibbs equation. The roughly estimated parameters of the kinetic model were then adjusted simultaneously to minimize the error on CO_2 conversion and CH_4 and CO selectivities at 623 K, 673 K and 723 K.

3. Results

3.1. CO_2 methanation

The CO_2 methanation rate dependence on reactants and products partial pressure has been established at different temperatures with 1.5 mg of Ni/Al_2O_3 catalyst diluted in SiC ($\Psi = 32$). The rate of CH_4 formation is highly dependent on the H_2 concentration (Figure 3 (a) at 22 kPa CO_2 partial pressure) whereas it is weakly dependent on the CO_2 partial pressure (Figure 3 (b) at 55 kPa H_2 partial pressure). No significant influence of CH_4 partial pressure on CH_4 formation rate is detected (Figure 3 (c) at 55 kPa H_2 partial pressure and 22 kPa CO_2 partial pressure) whereas an inhibition by water pressure is observed in Figure 3 (d).

3.2. RWGS

The effect of CO_2, H_2, H_2O and CH_4 partial pressures on the CO formation rate associated with the RWGS reaction was studied on 1.5 mg Ni/Al_2O_3 catalyst diluted in SiC ($\Psi = 32$). No dependence on the H_2 concentration is visible (Figure 4 (a) at 22 kPa CO_2 partial pressure) whereas the rate of CO formation is highly dependent on the CO_2 concentration (Figure 4 (b) at 55 kPa H_2 partial pressure). No influence

of CH_4 partial pressure and an inhibition by water pressure (Figure 4 (c) and (d)) are observed at 55 kPa H_2 partial pressure and 22 kPa CO_2 partial pressure.

The effect of CO partial pressure has been investigated on the CO_2 formation rate associated with the WGS reaction (reverse reaction of Eq (2)), *i.e.* with a flow of CO/H_2O at the entry of the reactor to avoid the competition with methanation reactions. CO_2 formation rate is moderately dependent on CO partial pressure (Figure 5 at 20 kPa H_2O partial pressure).

3.3. CO methanation

The CO methanation rate dependence on reactants partial pressure was determined at 623 K, 673 K and 723 K. A quasi linear dependence on the H_2 partial pressure (Figure 6 (a) at 25 kPa CO partial pressure) was observed whereas the dependence on CO is much weaker (Figure 6 (b) at 40 kPa H_2 partial pressure).

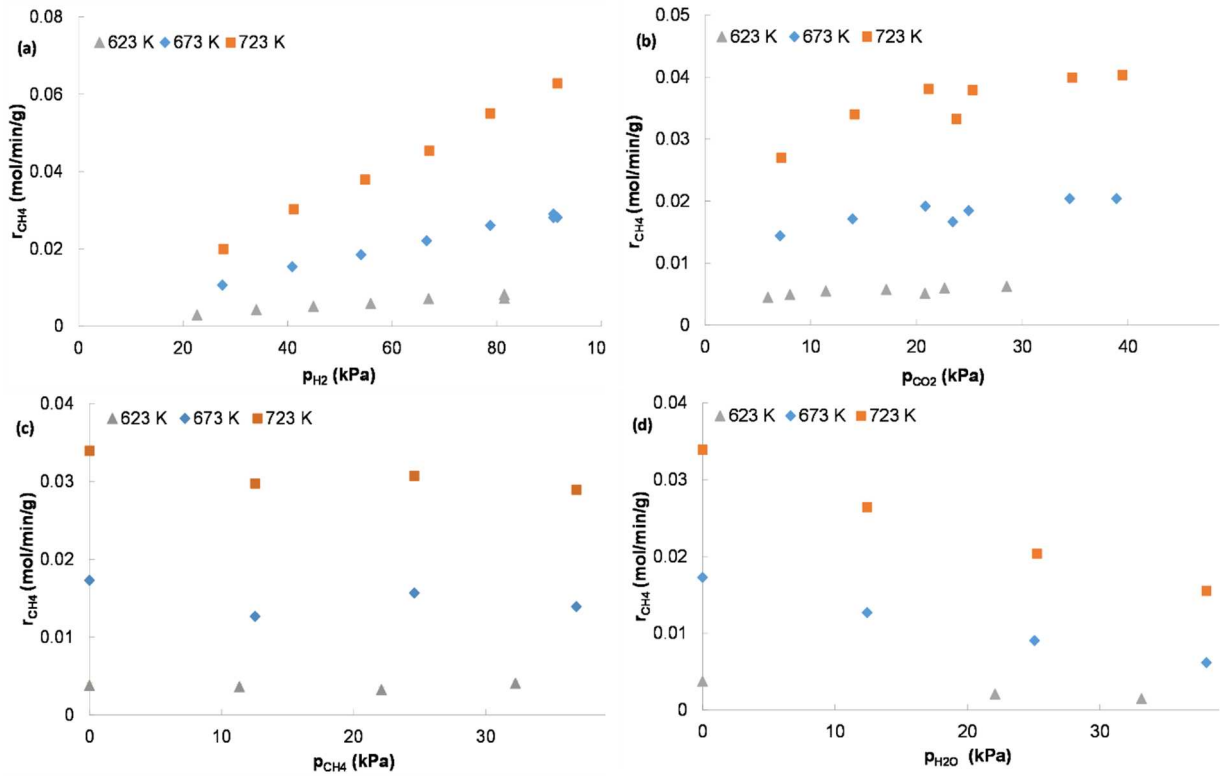

Figure 3 : Effect of partial pressure on CO_2 methanation on 1.5 mg Ni/Al_2O_3 catalyst diluted in SiC, 115 kPa total pressure and 1.06 10^6 h^{-1} at 623 K – 130 kPa total pressure and 3.16 10^6 h^{-1} at 673 K and 723 K: (a) H_2 at 22 kPa CO_2 partial pressure; (b) CO_2 at 55 kPa H_2 partial pressure; (c) CH_4 and (d) H_2O at 55 kPa H_2 partial pressure and 22 kPa CO_2 partial pressure

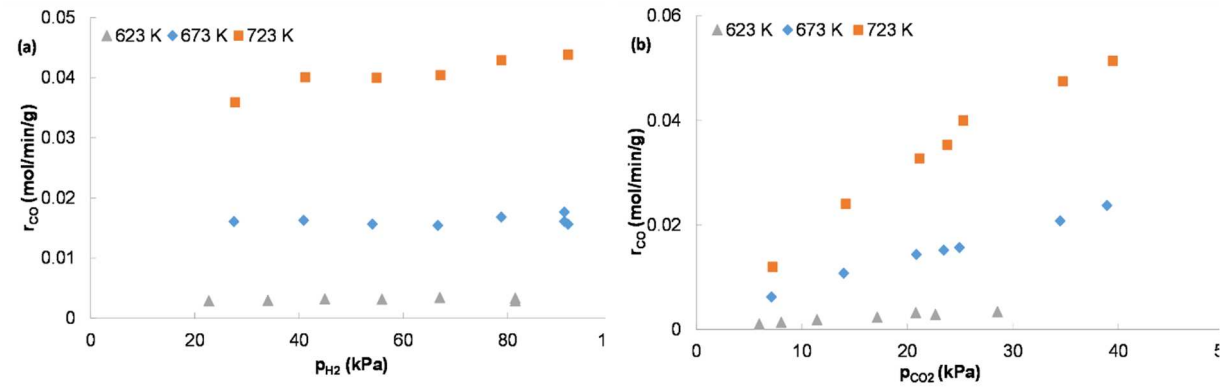

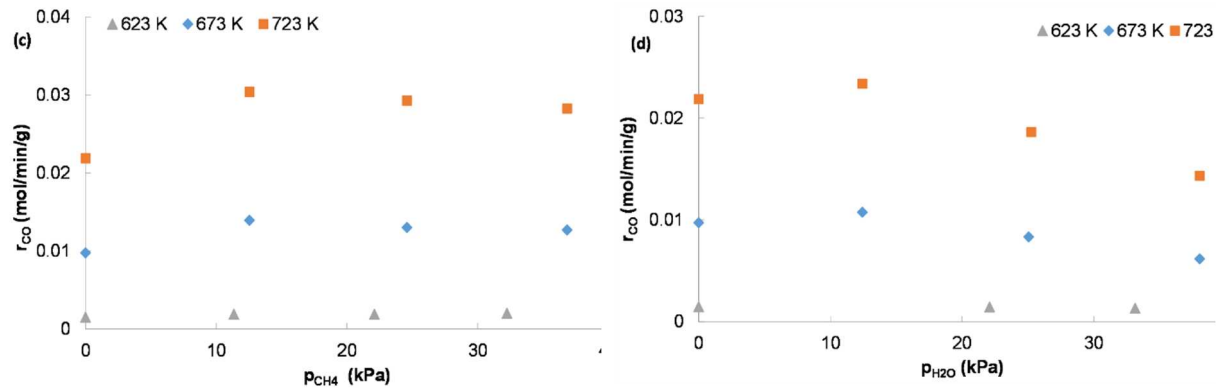

Figure 4 : Effect of partial pressure on RWGS on 1.5 mg Ni/Al_2O_3 catalyst diluted in SiC, 115 kPa total pressure and 1.06 10^6 h^{-1} at 623 K – 130 kPa total pressure and 3.16 10^6 h^{-1} at 673 K and 723 K: (a) H_2 at 22 kPa CO_2 partial pressure; (b) CO_2 at 55 kPa H_2 partial pressure; (c) CH_4 and (d) H_2O at 55 kPa H_2 partial pressure and 22 kPa CO_2 partial pressure

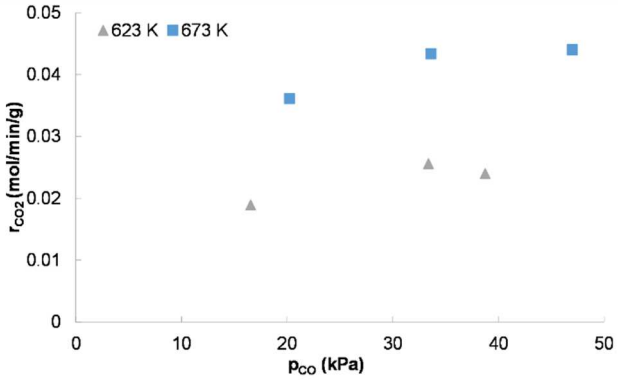

Figure 5 : CO partial pressure dependence on WGS on 1.5 mg Ni/Al_2O_3 catalyst diluted in SiC, 20 kPa H_2O partial pressure, 115 kPa total pressure and 1.06 10^6 h^{-1} at 623 K – 140 kPa total pressure and 3.16 10^6 h^{-1} at 673 K

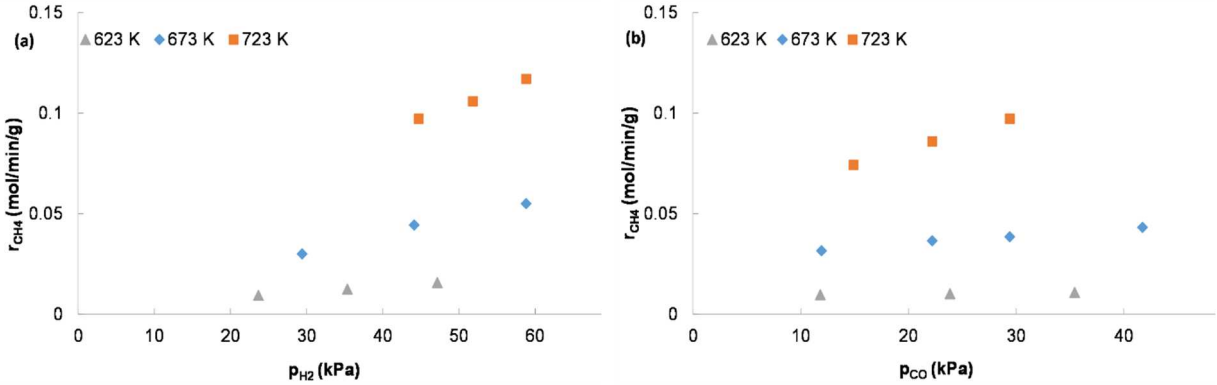

Figure 6 : (a) H_2 partial pressure dependence at 25 kPa CO partial pressure, and (b) CO partial pressure dependence at 40 kPa H_2 partial pressure on CO methanation on 1.5 mg Ni/Al_2O_3 catalyst diluted in SiC, 118 kPa total pressure and 1.66 10^6 h^{-1} at 623 K – 148 kPa total pressure and 5.0 10^6 h^{-1} at 673 K and 723 K

4. Discussion

The main rate expressions for CO_2 methanation, CO methanation and RWGS commonly used in literature are listed in Table 1. Simplification of these kinetic models in different situations presented below are tested and compared with experimental results obtained at low conversion (below 20%).

Table 1 : Literature rate expressions for CO_2 methanation, CO methanation and RWGS (including reverse reaction)

CO_2 methanation rate equations		
Xu and Froment [13]	$r_{CO_2\ meth} = \frac{k_{CO_2\ meth}\, p_{H_2}^{0.5} p_{CO_2} \left(1 - \frac{p_{H_2O}^2 P_{CH_4}}{p_{H_2}^4 p_{CO_2} K_{eq,CO_2\ meth}}\right)}{\left(1 + K_{CO} p_{CO} + K_{H_2} p_{H_2} + K_{CH_4} p_{CH_4} + K_{H_2O} \frac{p_{H_2O}}{p_{H_2}}\right)^2}$	(5)
Bartholomew [15]	$r_{CO_2\ meth} = \frac{k_{CO_2\ meth} p_{CO_2}^{0.5} p_{H_2}^{0.5} \left(1 - \frac{p_{H_2}^4 p_{CO_2}}{p_{H_2O}{}^2 p_{CH_4} K_{eq,CO_2\ meth}}\right)}{\left(1 + K_1 (p_{CO_2}/p_{H_2})^{0.5} + K_2 (p_{CO_2} p_{H_2})^{0.5} + p_{CO}/K_3\right)^2}$	(6)
RWGS rate equations		
Xu and Froment [13]	$r_{RWGS} = \frac{k_{RWGS} p_{CO_2} \left(1 - \frac{p_{H_2O} p_{CO}}{p_{H_2} p_{CO_2} K_{eq,RWGS}}\right)}{\left(1 + K_{CO} p_{CO} + K_{H_2} p_{H_2} + K_{CH_4} p_{CH_4} + K_{H_2O} \frac{p_{H_2O}}{p_{H_2}}\right)^2}$	(7)
Wheeler [25]	$r_{RWGS} = \frac{k_{RWGS} K_{H_2} K_{CO_2} p_{H_2} p_{CO_2} \left(1 - \frac{p_{H_2O} p_{CO}}{p_{H_2} p_{CO_2} K_{eq,RWGS}}\right)}{\left(1 + K_{CO} p_{CO} + K_{H_2O} p_{H_2O} + K_{CO_2} p_{CO_2} + K_{H_2} p_{H_2}\right)^2}$	(8)
CO methanation rate equations		
Xu and Froment [13]	$r_{CO\ meth} = \frac{k_{CO\ meth} p_{H_2}^{0.5} p_{CO} \left(1 - \frac{p_{H_2O} p_{CH_4}}{p_{H_2}^3 P_{CO} K_{eq,CO\ meth}}\right)}{\left(1 + K_{CO} p_{CO} + K_{H_2} p_{H_2} + K_{CH_4} p_{CH_4} + K_{H_2O} \frac{p_{H_2O}}{p_{H_2}}\right)^2}$	(9)

4.1. CO_2 methanation rate equation

The Xu and Froment kinetic model [13] simplifies as follows at low conversion with a CO_2/H_2 feed (as p_{CO}, p_{CH_4}, and p_{H_2O} are negligible):

$$r_{meth\ CO_2} = \frac{k_{CO_2\ meth} p_{CO_2} p_{H_2}^{0.5}}{\left(1 + K_{H_2} p_{H_2}\right)^2} \quad (10)$$

However, the proportionality between the CO_2 methanation reaction rate and the CO_2 partial pressure is not obtained experimentally (Figure 7). This model is therefore rejected.

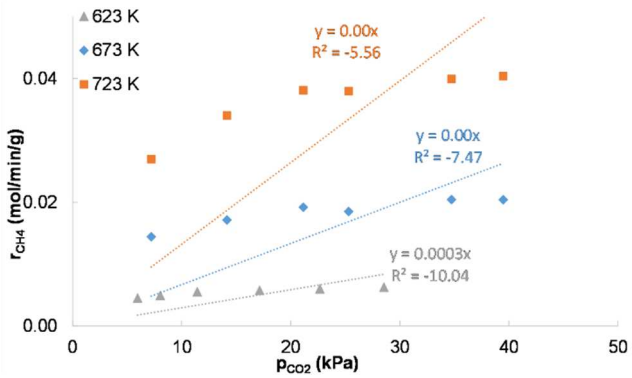

Figure 7 : Xu and Froment linear model of the CO_2 methanation (lines) according to p_{CO_2} vs experimental data (points) at 623 K, 673 K and 723 K (low conversion)

The model proposed by Weatherbee and Bartholomew [15] was also tested. The same method of simplification was applied at low conversion and led to the following expression with a CO_2/H_2 feed:

$$r_{CO_2\ meth} = \frac{k_{CO_2\ meth} p_{CO_2}^{0.5} p_{H_2}^{3/2}}{\left(p_{H_2}^{0.5} + K_1 p_{CO_2}^{0.5} + K_2 p_{H_2} p_{CO_2}^{0.5}\right)^2} \quad (11)$$

The validity of this model is verified by linearization of (11). In Figure 8 (a) at 55 kPa H_2 partial pressure, straight lines are obtained as a function of $\left(p_{CO_2}\right)^{0.5}$ while plotting $\left(p_{CO_2}^{0.25}/r_{CO_2\ meth}^{0.5}\right)$ at 623 K, 673 K and 723 K. However, in Figure 8 (b) at 22 kPa CO_2 partial pressure, plots of $\left(p_{H_2}^{0.75}/r_{CO_2\ meth}^{0.5}\right)$ with $\left(p_{H_2}\right)^{0.5}$ admit negative coefficients. This would implies that some adsorption or kinetic constants are negative which is not consistent and leads to the rejection of this model.

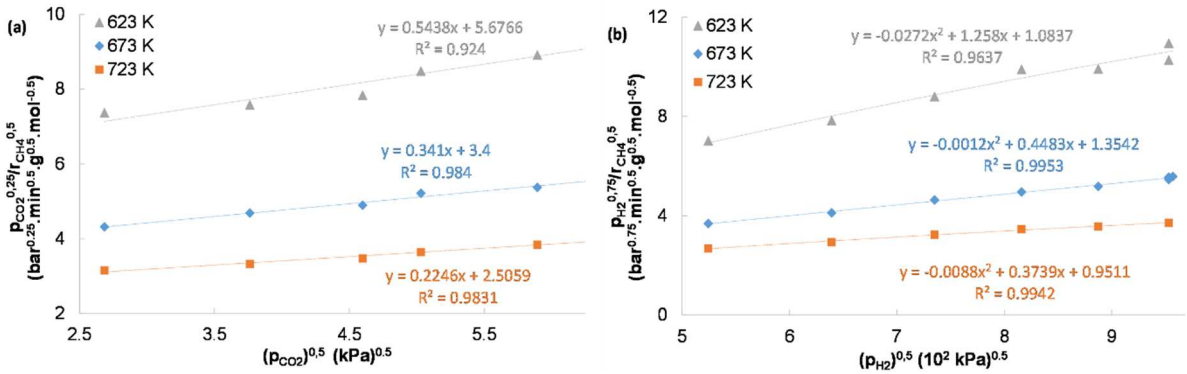

Figure 8 : Bartholomew linear function (a) according to p_{CO_2} and (b) according to p_{H_2} at low CO_2 methanation conversion

The simple kinetic model proposed by Wheeler *et al.* (Eq.(8)) and identified for the WGS reaction [25] is adapted for the CO_2 methanation reaction. In the case of a CO_2/H_2 feed, at low CO_2 conversion, the equation becomes:

$$r_{CO_2\ meth} = \frac{k_{CO_2\ meth} K_{H_2} K_{CO_2} p_{H_2} p_{CO_2}}{\left(1 + K_{CO_2} p_{CO_2} + K_{H_2} p_{H_2}\right)^2} \quad (12)$$

Linearization of the kinetics leads to plot $\left(p_{CO_2}/r_{CO_2\ meth}\right)^{0.5}$ as a function of p_{CO_2} at constant p_{H_2} and $\left(p_{H_2}/r_{CO_2\ meth}\right)^{0.5}$ as a function of p_{H_2} at constant p_{CO_2}. A good fit of the experimental results for linear functions are obtained in both Figure 9 (a) at 55 kPa H_2 partial pressure and (b) at 22 kPa CO_2 partial pressure at 623 K, 673 K and 723 K. The mechanism behind this equation assumes a bimolecular limiting step: $CO_2X + H_2X \rightarrow COX + H_2OX$, where X is a vacant site on the metal surface [25]. The H_2 and CO_2 adsorption constants, and the CO_2 methanation kinetic constant are identified from the slope and intercept of the regression lines of Figure 9 (a) and (b). The identified constants model correctly the CH_4 formation rate at the three temperatures (Figure 10 (a) and (b)).

The inhibition by water (Figure 3 (d)) is accounted for by adding in the adsorption term the H_2O partial pressure modulated by an adsorption constant, meaning an adsorption competition on the available active sites. The reaction rate expression at low conversion for a $CO_2/H_2/H_2O$ feed is thus the following:

$$r_{CO_2\ meth} = \frac{k_{CO_2\ meth} K_{H_2} K_{CO_2} p_{H_2} p_{CO_2}}{\left(1 + K_{CO_2} p_{CO_2} + K_{H_2} p_{H_2} + K_{H_2O} p_{H_2O}\right)^2} \quad (13)$$

H_2O adsorption constant is identified at 623 K, 673 K and 723 K on the experimental data of Figure 3 (d). The H_2O inhibition model fits well the CH_4 formation rate data (Figure 10 (c)).

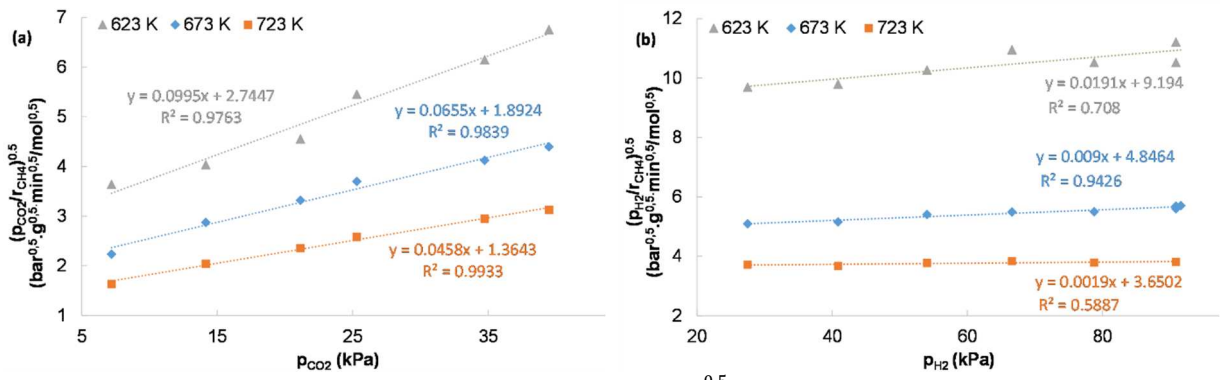

Figure 9 : Plot of the adapted Wheeler linear function $\left(p_i/r_{meth\ CO_2}\right)^{0.5}$ versus p_i at low CO_2 methanation conversion (a) i = CO_2 at 55 kPa H_2 partial pressure and (b) i = H_2 at 22 kPa CO_2 partial pressure

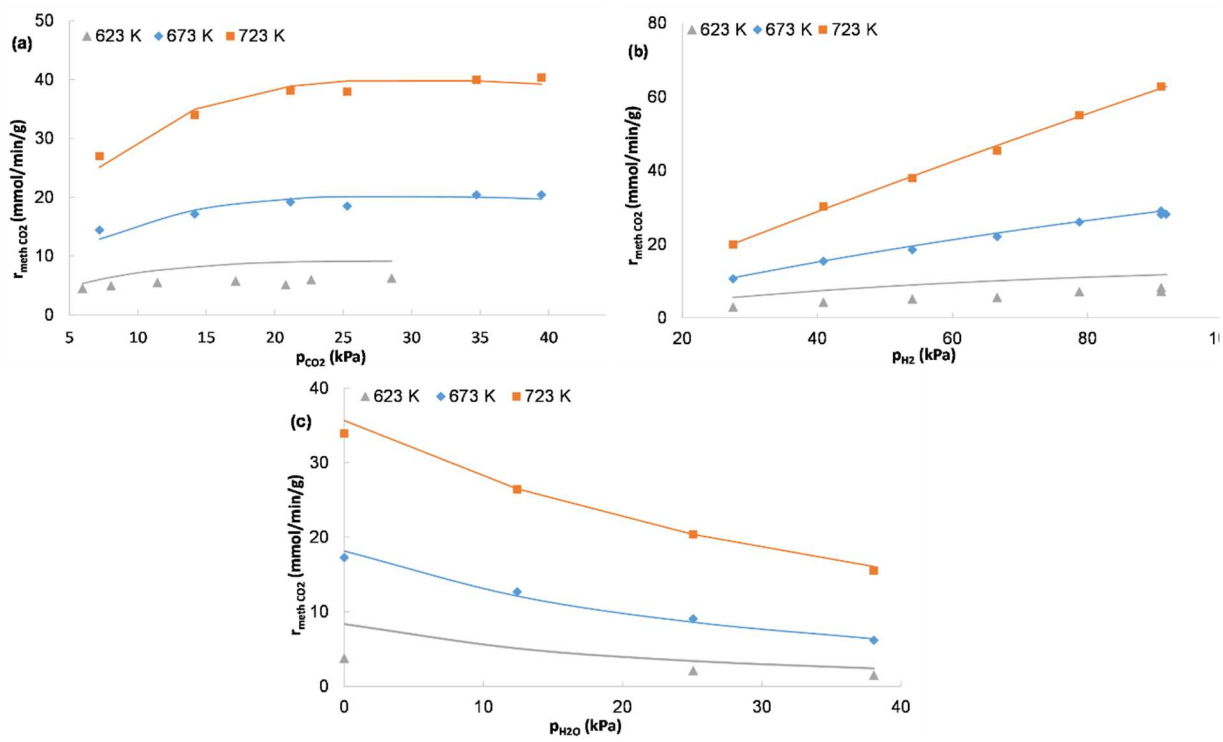

Figure 10 : Comparison between the CH_4 formation rate experimental results (points) and the CO_2 methanation rate equation predicted by the adapted Wheeler model at low conversion (continuous line) at 623 K, 673 K and 723 K: (a) Effect of CO_2 partial pressure at 55 kPa H_2 partial pressure, (b) Effect of H_2 partial pressure at 22 kPa CO_2 partial pressure, (c) Effect of H_2O partial pressure at 55 kPa H_2 partial pressure and 22 kPa CO_2 partial pressure

4.2. RWGS rate equation

According to our results, RWGS is not influenced by hydrogen partial pressure (Figure 4 (a)). The following model is proposed at low CO_2 conversion with a CO_2/H_2 feed assuming CO_2 dissociative adsorption as limiting step: $CO_2 + X \rightarrow CO + OX$ [26,27] and tested on the CO formation rate data:

$$r_{RWGS} = \frac{k_{RWGS} K_{CO_2} p_{CO_2}}{\left(1 + K_{H_2} p_{H_2} + K_{CO_2} p_{CO_2}\right)} \quad (14)$$

The validity of this model is verified by linearization of (14). In Figure 11, at 55 kPa H_2 partial pressure, straight lines are obtained as a function of p_{CO_2} while plotting (p_{CO_2}/r_{RWGS}) at 623 K, 673 K and 723 K.

Keeping the value of adsorption constants previously determined in the CO_2 methanation study, the resolution gives the RWGS kinetic constant to model the CO formation rate at 623 K, 673 K and 723 K (Figure 12):

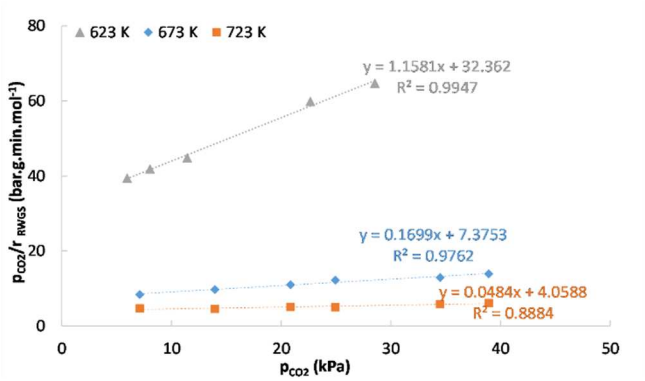

Figure 11 : Plot of the proposed RWGS linear model $p_{CO_2}/r_{meth\ CO_2}$ versus p_{CO_2} at low CO_2 conversion and 55 kPa H_2 partial pressure

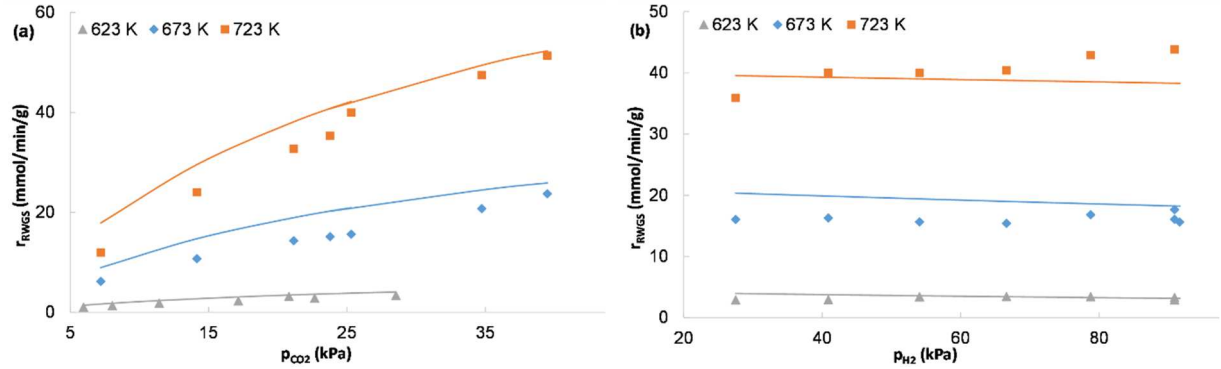

Figure 12 : Comparison between the CO formation rate experimental results (points) and the RWGS rate equation predicted by the adapted model at low conversion (continuous line) at 623 K, 673 K and 723 K: (a) Effect of CO_2 partial pressure at 55 kPa H_2 partial pressure and (b) Effect of H_2 partial pressure at 22 kPa CO_2 partial pressure

4.3. CO methanation rate equation

Linearization of the Xu and Froment kinetics at low conversion with a CO/H_2 feed leads to plot $(p_{CO}^{0.25}/r_{CO\ meth}^{0.5})$ as a function of p_{H_2} at constant p_{CO}. However, results are not presented here because negative coefficients are obtained.

Based on the results of the CO_2 methanation kinetic study (Eq (12)), the following model is proposed in the case of a low conversion CO methanation reaction with a CO/H_2 feed:

$$r_{CO\ meth} = \frac{k_{CO\ meth} K_{H_2} K_{CO} p_{H_2} p_{CO}}{\left(1 + K_{H_2} p_{H_2} + K_{CO} p_{CO}\right)^2} \qquad (15)$$

Linearization of the kinetics leads to plot $(p_{CO}/r_{CO\ meth})^{0.5}$ as a function of p_{CO} at constant p_{H_2} and $\left(p_{H_2}/r_{CO\ meth}\right)^{0.5}$ as a function of p_{H_2} at constant p_{CO}. A good fit of the experimental results for linear functions are obtained in both Figure 13 (a) at 40 kPa H_2 partial pressure and (b) at 25 kPa CO partial pressure at 623 K, 673 K and 723 K. The CO methanation kinetic constant as well as the CO adsorption constant are identified from the slope and intercept of the regression lines of Figure 13 (a) and (b) knowing the H_2 adsorption constant from the CO_2 methanation rate equation study. The identified model fits adequately the CH_4 formation rate data (Figure 14 (a) and (b)).

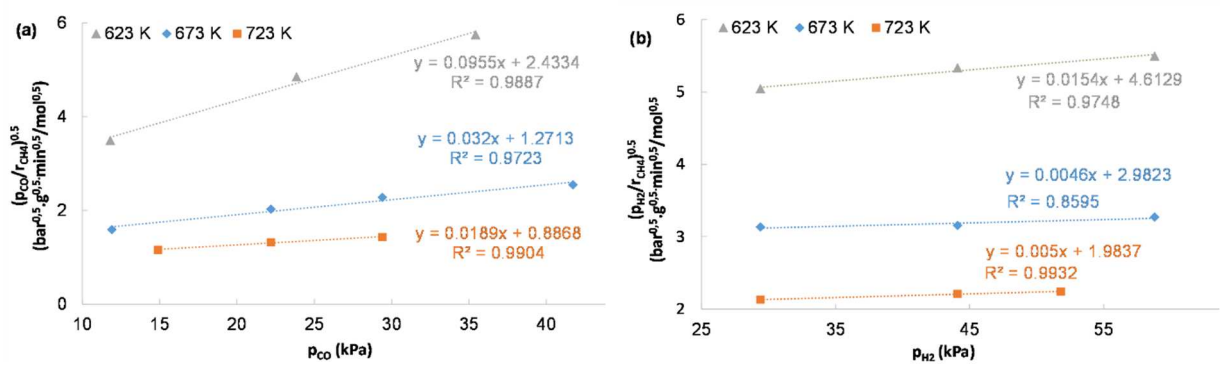

Figure 13 : Plot of the adapted linear function $(p_i/r_{meth\,CO})^{0.5}$ versus p_i at low CO methanation conversion (a) i = CO at 40 kPa H_2 partial pressure; (b) i = H_2 at 25 kPa CO_2 partial pressure

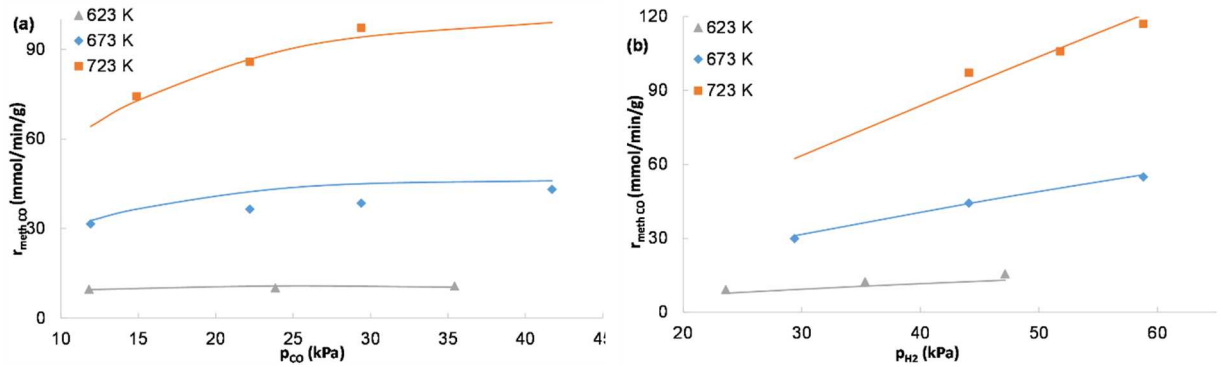

Figure 14 : Comparison between the CH_4 formation rate experimental results (points) and the CO methanation rate equation predicted by the adapted model at low conversion (continuous line) at 623 K, 673 K and 723 K: (a) Effect of CO partial pressure at 40 kPa H_2 partial pressure and (b) Effect of H_2 partial pressure at 25 kPa CO_2 partial pressure

4.4. Parameters adjustment

The kinetic experiments performed at low conversion (below 20% for all reactive components) allowed to determine the form of the three reaction rates (Eqs (1), (2) and (3)) as well as a first identification of the kinetic and adsorption parameters. The thermodynamic limitations were added to the kinetics established at low conversion in order to consider the global reaction rate of the balanced reaction:

$$r_{global} = r^+ - r^- = r^+\left(1 - \frac{Q_r}{K_{eq}}\right)$$

Moreover, the adsorption of all species likely to compete significantly on the catalyst active sites (*i.e.* H_2, CO_2, H_2O, and CO) was taken into account. The obtained equations are given in Table 2.

Table 2 : Kinetic model of this study

CO_2 methanation rate equations	
$r_{CO_2\,meth} = \dfrac{k_{CO_2\,meth}K_{H_2}K_{CO_2}p_{H_2}p_{CO_2}\left(1 - \dfrac{p_{CH_4}p_{H_2O}^2}{p_{H_2}^4\,p_{CO_2}K_{eq,CO_2\,meth}}\right)}{\left(1 + K_{CO_2}p_{CO_2} + K_{H_2}p_{H_2} + K_{H_2O}p_{H_2O} + K_{CO}p_{CO}\right)^2}$	(16)
RWGS rate equations	
$r_{RWGS} = \dfrac{k_{RWGS}K_{CO_2}p_{CO_2}\left(1 - \dfrac{p_{CO}p_{H_2O}}{p_{H_2}\,p_{CO_2}K_{eq,RWGS}}\right)}{(1 + K_{CO_2}p_{CO_2} + K_{H_2}p_{H_2} + K_{H_2O}p_{H_2O} + K_{CO}p_{CO})}$	(17)

CO methanation rate equations

$$r_{CO\ meth} = \frac{k_{CO\ meth} K_{H_2} K_{CO} p_{H_2} p_{CO} \left(1 - \frac{p_{CH_4} p_{H_2O}}{p_{H_2}^3\ p_{CO} K_{eq,CO\ meth}}\right)}{\left(1 + K_{CO_2} p_{CO_2} + K_{H_2} p_{H_2} + K_{H_2O} p_{H_2O} + K_{CO} p_{CO}\right)^2} \quad (18)$$

For a separated set of experiments (described in 2.4), an isothermal plug flow model was used to integrate the three reactions occurring in parallel. As the three reaction rates include three kinetic constants and four adsorption constants, a total of 14 parameters are involved in the rate equations. The adjustments were first performed on the kinetic constants and the adsorption constants at 673 K. This allowed to first reduce the number of parameters from 14 to 7 while keeping a physical meaning when adjusting parameters.

Experimental and theoretical CO_2 conversion and CH_4 and CO selectivities are plotted as a function of an equivalent mass of catalyst defined by:

$$equivalent\ mass = real\ mass \frac{reference\ flow\ rate}{real\ flow\ rate}$$

A reference flow rate, being arbitrary fixed at 100 ml (STP) min^{-1}, is used to link the experimental results (with different mass and flow rates) to the modeled values.

First, reaction rates expressions were simplified by introducing apparent kinetic constants as follows:

$$k_{app,CO_2\ meth} = k_{CO_2\ meth} K_{CO_2} K_{H_2} \quad (19)$$

$$k_{app,RWGS} = k_{RWGS} K_{CO_2} \quad (20)$$

$$k_{app,CO\ meth} = k_{CO\ meth} K_{CO} K_{H_2} \quad (21)$$

The aim of this mathematical operation is to avoid the influence of adsorption parameters on both numerator and denominator.

With a H_2/CO_2 feed, the CO_2 methanation and the RWGS are both primary reactions whereas the CO methanation is a secondary reaction. Hence, for each temperature, the ratio between CH_4 and CO selectivities extrapolated at equivalent mass of zero corresponds to the ratio of CO_2 methanation over RWGS initial rates. The obtained ratio allowed to link kinetic constants of CO_2 methanation to RWGS reaction. The number of parameters is thus declined to 6.

As conversion at relatively low equivalent mass is not sensitive to secondary reaction, conversion was then adjusted by tuning RWGS kinetic constant (and so CO_2 methanation automatically with).
Furthermore, the kinetic constant of the CO methanation was adjusted by adjusting CO selectivities in the whole range of equivalent mass.

The adsorption constants were then modified in the denominator of the rate equations to fit the form of the curve of CO_2 conversion and CH_4 and CO selectivities (*i.e.* inhibit more or less the reaction rates). Based on the roughly estimated parameters, the influence of the CO adsorption constant on the reaction rates is much weaker than the ones of the three other compounds involved (CO_2, H_2 and H_2O), this parameter was thus not changed.

Once the adsorption parameters modified, the sequence was repeated iteratively until good fits were obtained at a given temperature. The procedure was then repeated for the 2 other temperatures with the constraint of acceptable Arrhenius plots for each of the 7 kinetic and adsorption constants.

Comparison of the experimental and theoretical CO_2 conversions and CH_4 and CO selectivities at 623, 673 and 723 K are presented in Figure 15 for the adjusted parameters. As the obtained error is small at the three temperatures, the adjusted apparent kinetic constants allowed to calculate real kinetic constants present in Eqs (16), (17) and (18).

The final parameters given in Table 3 predict with an accuracy of 20% the CH_4 formation rate (Figure 16) for the three temperatures and conversion rates ranging from 5% to 75%.

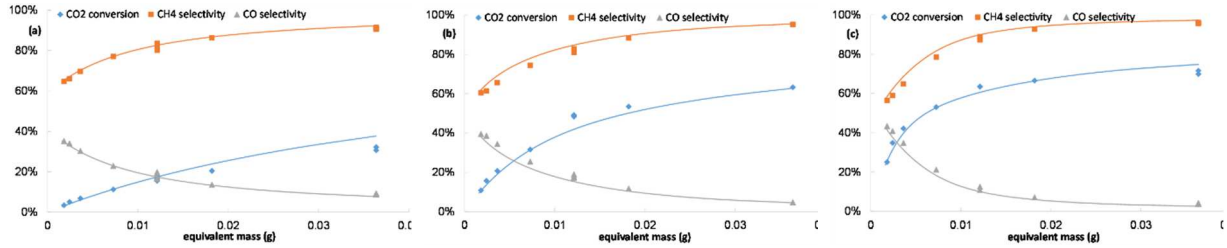

Figure 15: CO_2 conversion and CH_4 and CO selectivities of an isothermal plug flow reactor for a molar ratio $H_2/CO_2/N_2$ = 74/17/9 – continuous line: model – point: experimental value: (a) at 623 K; (b) at 673 K and (c) at 723 K

Table 3 : Final parameters of the kinetic model following an Arrhenius law for the kinetic constants and as Van't Hoff type for the adsorption constants

		K_{CO}	K_{H2O}	K_{CO2}	K_{H2}
Adsorption constants	Q (kJ mol^{-1})	40.6	14.5	9.72	52.0
	K_0 (bar^{-1})	2.39 10^{-3}	6.09 10^{-1}	1.07	5.20 10^{-5}

		$k_{CO_2\ meth}$	k_{RWGS}	$k_{CO\ meth}$
Kinetic constants	Ea (kJ mol^{-1})	110	97.1	97.3
	k_0 (mol min^{-1} g^{-1})	1.14 10^8	1.78 10^6	2.23 10^8

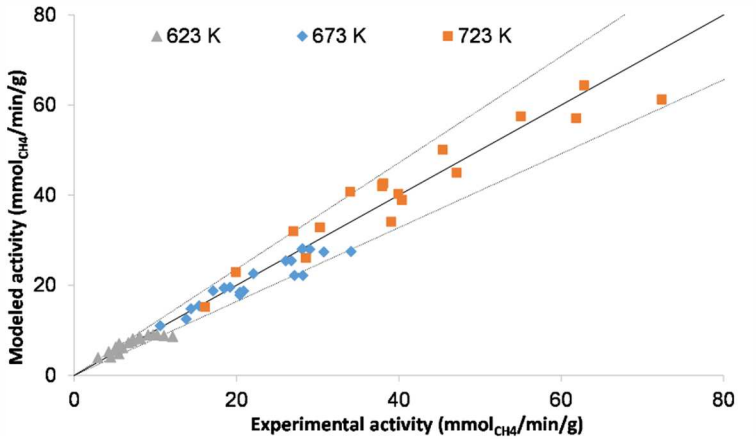

Figure 16: Parity plot of the experimental and modeled CH_4 activity within 20% error at 623 K, 673 K and 723 K - $H_2/CO_2/N_2$ at the reactor inlet (data taken from experiments at low conversion and parameters adjustment experiments)

5. Conclusion

An intrinsic kinetic model was proposed to represent both the direct and indirect paths of the CO_2 methanation reaction (*i.e.* CO_2 methanation and Reverse Water Gas Shift + CO methanation) between 623 K and 723 K, at atmospheric pressure.

First, the partial pressure rate dependence of each component was established on each reaction, at different temperatures to select the form of the three kinetic laws and to identify the kinetic and adsorption parameters. For these tests, the CO_2 conversion (CO conversion) was limited to 20% in order to consider only the direct direction of the CO_2 methanation and RWGS (CO methanation).

Then, these parameters were adjusted by minimizing the error between the CO_2 conversion and CH_4 and CO selectivities predicted by an isothermal plug-flow model and several tests at higher conversion rate at 623 K, 673 K and 723 K. An excellent fit was obtained allowing the prediction of the CH_4 formation rate within 20% error.

Future works will include a kinetic model validation at the CO_2 methanation milli-structured fixed-bed reactor-exchanger scale. The final purpose will be the prediction of the catalyst activity over time on stream inside the CO_2 methanation reactor using the kinetic model of this study coupled with a deactivation model.

Acknowledgments

This work was supported by the French Environment and Energy Management Agency (ADEME), French Alternative Energies and Atomic Energy Commission (CEA) and ATMOSTAT. It is the result of experiments conducted at the ICPEES Laboratory in Strasbourg.

Nomenclature

Ea	Activation energy (J mol^{-1})
F	Molar flow (mol min^{-1})
GHSV	Gas Hourly Space Velocity (h^{-1})
k_j	Reaction rate constant of reaction j (mol min^{-1} g^{-1})
k_0	Pre-exponential factor of rate constant (mol min^{-1} g^{-1})
K_i	Adsorption equilibrium constant of constituent i (bar^{-1})
K_0	Pre-exponential factor for adsorption equilibrium constant (bar^{-1})
$K_{eq,j}$	Equilibrium constant of reaction j
p_i	Partial pressure of constituent i
Q	Heat of adsorption (J mol^{-1})
Q_r	Reaction quotient (-)
r_j	Reaction rate of reaction j
r_{CH_4}	Reaction rate of methane formation (mol min^{-1} g^{-1})
r_{CO}	Reaction rate of CO formation (mol min^{-1} g^{-1})
r_{global}	Global reaction rate (mol min^{-1} g^{-1})
r^+	Direct reaction rate (mol min^{-1} g^{-1})
r^-	Reverse reaction rate (mol min^{-1} g^{-1})
R	Ideal gas constant (R = 8.314 J mol^{-1} K^{-1})
T	Temperature (K)
Greek letters	
$\Delta_r H$	Heat of reaction (J mol^{-1})
Ψ	Inert dilution factor ($\Psi = \mathrm{m_{SiC}}/m_{catalyst}$)

Appendices

Supplementary material related to the theoretical heat and mass transfer limitations verifications is available.

References

[1] M.A.A. Aziz, A.A. Jalil, S. Triwahyono, A. Ahmad, CO_2 methanation over heterogeneous catalysts: recent progress and future prospects, Green Chem. 17 (2015) 2647–2663. doi:10.1039/C5GC00119F.

[2] P. Frontera, A. Macario, M. Ferraro, P. Antonucci, Supported Catalysts for CO_2 Methanation: A Review, Catalysts. 7 (2017) 59. doi:10.3390/catal7020059.
[3] J. Gao, Q. Liu, F. Gu, B. Liu, Z. Zhong, F. Su, Recent advances in methanation catalysts for the production of synthetic natural gas, RSC Adv. 5 (2015) 22759–22776. doi:10.1039/C4RA16114A.
[4] M. Götz, J. Lefebvre, F. Mörs, A. McDaniel Koch, F. Graf, S. Bajohr, R. Reimert, T. Kolb, Renewable Power-to-Gas: A technological and economic review, Renew. Energy. 85 (2016) 1371–1390. doi:10.1016/j.renene.2015.07.066.
[5] Y. Li, S.H. Chan, Q. Sun, Heterogeneous catalytic conversion of CO_2 : a comprehensive theoretical review, Nanoscale. 7 (2015) 8663–8683. doi:10.1039/C5NR00092K.
[6] S. Rönsch, J. Schneider, S. Matthischke, M. Schlüter, M. Götz, J. Lefebvre, P. Prabhakaran, S. Bajohr, Review on methanation – From fundamentals to current projects, Fuel. 166 (2016) 276–296. doi:10.1016/j.fuel.2015.10.111.
[7] W. Wang, S. Wang, X. Ma, J. Gong, Recent advances in catalytic hydrogenation of carbon dioxide, Chem. Soc. Rev. 40 (2011) 3703. doi:10.1039/c1cs15008a.
[8] J. Sabatier, P. Senderens, Nouvelles synthèses de méthane, Compt Rend. (1902) 514–516.
[9] J. Gao, Y. Wang, Y. Ping, D. Hu, G. Xu, F. Gu, F. Su, A thermodynamic analysis of methanation reactions of carbon oxides for the production of synthetic natural gas, RSC Adv. 2 (2012) 2358. doi:10.1039/c2ra00632d.
[10] P.J. Lunde, F.L. Kester, Carbon dioxide methanation on a ruthenium catalyst, Ind. Eng. Chem. Process Des. Dev. 13 (1974) 27–33.
[11] J.H. Chiang, J.R. Hopper, Kinetics of the hydrogenation of carbon dioxide over supported nickel, Ind. Eng. Chem. Prod. Res. Dev. 22 (1983) 225–228.
[12] R.E. Hayes, W.J. Thomas, K.E. Hayes, A study of the nickel-catalyzed methanation reaction, J. Catal. 92 (1985) 312–326.
[13] J. Xu, G.F. Froment, Methane steam reforming, methanation and water-gas shift: I. Intrinsic kinetics, AIChE J. 35 (1989) 88–96.
[14] J. Ducamp, A. Bengaouer, P. Baurens, Modelling and experimental validation of a CO_2 methanation annular cooled fixed-bed reactor exchanger, Can. J. Chem. Eng. 95 (2017) 241–252. doi:10.1002/cjce.22706.
[15] G.D. Weatherbee, C.H. Bartholomew, Hydrogenation of CO_2 on group VIII metals: II. Kinetics and mechanism of CO2 hydrogenation on nickel, J. Catal. 77 (1982) 460–472.
[16] F. Koschany, D. Schlereth, O. Hinrichsen, On the kinetics of the methanation of carbon dioxide on coprecipitated NiAl(O)x, Appl. Catal. B Environ. 181 (2016) 504–516. doi:10.1016/j.apcatb.2015.07.026.
[17] C.V. Miguel, A. Mendes, L.M. Madeira, Intrinsic kinetics of CO_2 methanation over an industrial nickel-based catalyst, J. CO2 Util. 25 (2018) 128–136. doi:10.1016/j.jcou.2018.03.011.
[18] A. Bengaouer, J. Ducamp, I. Champon, R. Try, Performance evaluation of fixed-bed, millistructured, and metallic foam reactor channels for CO_2 methanation, Can. J. Chem. Eng. 96 (2018) 1937–1945. doi:10.1002/cjce.23140.
[19] S. Danaci, L. Protasova, J. Lefevere, L. Bedel, R. Guilet, P. Marty, Efficient CO_2 methanation over Ni/Al_2O_3 coated structured catalysts, Catal. Today. 273 (2016) 234–243. doi:10.1016/j.cattod.2016.04.019.
[20] D. Schlereth, O. Hinrichsen, A fixed-bed reactor modeling study on the methanation of CO_2, Chem. Eng. Res. Des. 92 (2014) 702–712. doi:10.1016/j.cherd.2013.11.014.
[21] H. Gierman, Design of laboratory hydrotreating reactors: scaling down of trickle-flow reactors, Appl. Catal. 43 (1988) 277–286.
[22] D.E. Mears, The role of axial dispersion in trickle-flow laboratory reactors, Chem. Eng. Sci. 26 (1971) 1361–1366.
[23] C.F. Chu, K.M. Ng, Flow in packed tubes with a small tube to particle diameter ratio, AIChE J. 35 (1989) 148–158.
[24] S. Ergun, Fluid Flow through packed columns, Chem. Eng. Prog. 48 (1952) 89–92.
[25] C. Wheeler, The water–gas-shift reaction at short contact times, J. Catal. 223 (2004) 191–199. doi:10.1016/j.jcat.2004.01.002.
[26] M.S. Spencer, On the activation energies of the forward and reverse water-gas shift reaction, Catal. Lett. 32 (1995) 9–13.
[27] E.L. Fornero, D.L. Chiavassa, A.L. Bonivardi, M.A. Baltanás, Transient analysis of the reverse water gas shift reaction on Cu/ZrO_2 and Ga_2O_3 /Cu/ZrO_2 catalysts, J. CO2 Util. 22 (2017) 289–298. doi:10.1016/j.jcou.2017.06.002.

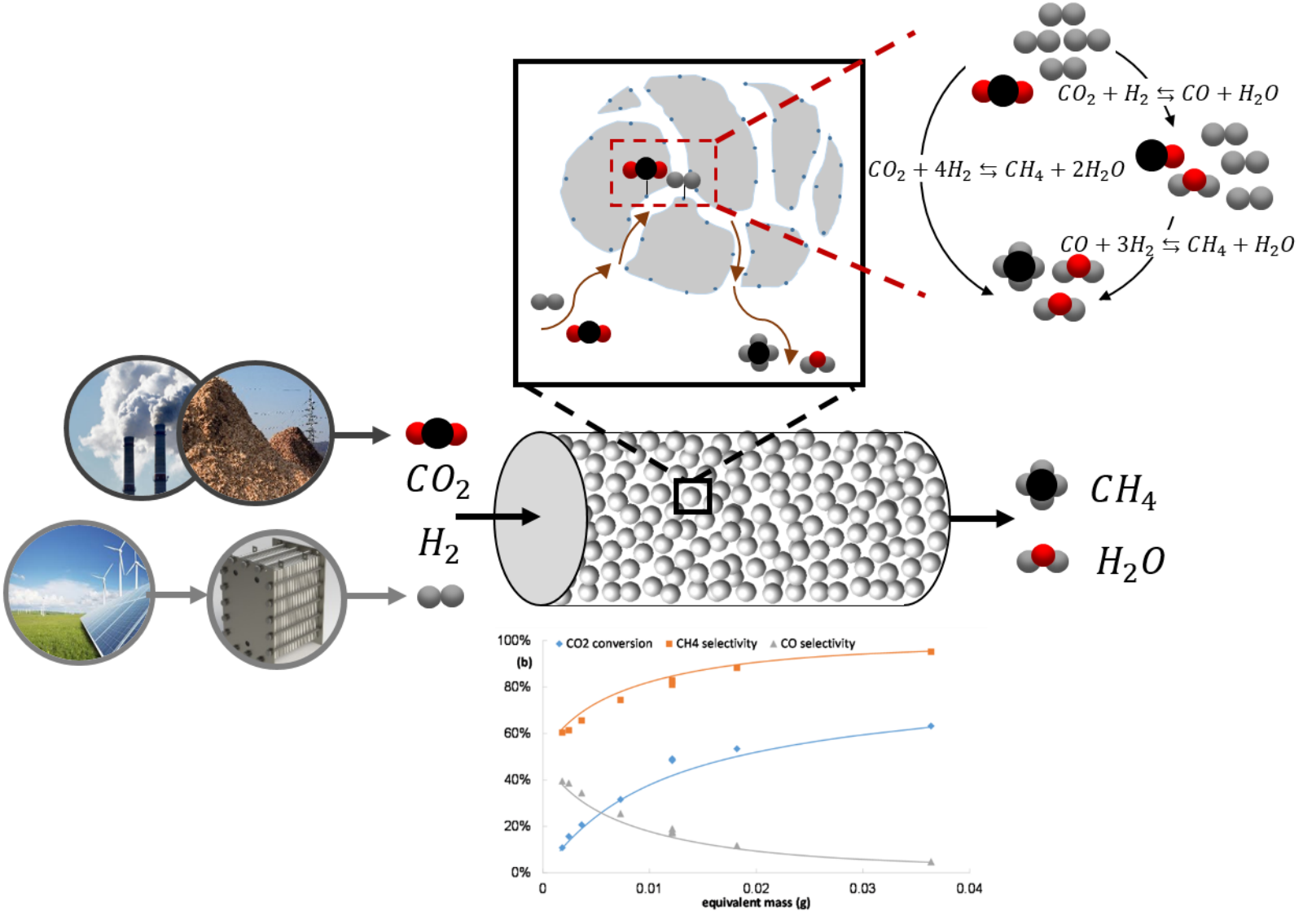
$CO_2 + H_2 \leftrightarrows CO + H_2O$
$CO_2 + 4H_2 \leftrightarrows CH_4 + 2H_2O$
$CO + 3H_2 \leftrightarrows CH_4 + H_2O$
CO_2
H_2
CH_4
H_2O
100%
(b)
80%
60%
40%
20%
0%
CO2 conversion
CH4 selectivity
CO selectivity
0
0.01
0.02
0.03
0.04
equivalent mass (g)